A Novel Role for the Immunoproteasome in Retinal Function

Stacy A. Hussong,[1,2] *Heidi Roehrich,*[3] *Rebecca J. Kapphahn,*[1] *Marcela Maldonado,*[1] *Machelle T. Pardue,*[4,5] *and Deborah A. Ferrington*[1,2]

Purpose. The immunoproteasome is a proteasome subtype with a well-characterized role in the immune system. The presence of high immunoproteasome concentrations in the photoreceptors and synaptic regions of the immune-privileged retina implies a role in visual transmission. In this study, immunoproteasome knockout (KO) mice lacking either one (*lmp7*$^{-/-}$, L7) or two (*lmp7*$^{-/-}$*/mecl-1*$^{-/-}$, L7M1) catalytic subunits of the immunoproteasome were used to test the hypothesis that it is essential for the maintenance of normal retinal function.

Methods. Wild-type (WT) and immunoproteasome KO mice lacking either one (L7) or two (L7M1) catalytic subunits of the immunoproteasome were studied to determine the importance of the immunoproteasome in maintaining normal retinal function and morphology. Changes in retinal morphology were assessed in mice 2 to 24 months of age. Retinal function was measured with electroretinography (ERG), and relative content of select retinal proteins was assessed by immunoblot analysis.

Results. Retinal morphometry showed no major abnormalities in age-matched WT or KO mice. No significant difference was observed in the levels of proteins involved in vision transmission. ERGs from KO mice exhibited an approximate 25% decrease in amplitude of the dark- and light-adapted b-waves and faster dark-adapted b-wave implicit times.

Conclusions. Immunoproteasome deficiency causes defects in bipolar cell response. These results support a previously unrecognized role for the immunoproteasome in vision transmission. (*Invest Ophthalmol Vis Sci.* 2011;52:714–723) DOI:10.1167/iovs.10-6032

The proteasome proteolytic complex plays a fundamental role in processes essential for cell viability, such as cell cycle regulation, control of signal transduction and gene expression, and the degradation of oxidized and misfolded proteins.[1,2] The 20S catalytic core of the proteasome is a barrel-shaped structure, consisting of four heptameric rings. The two outer rings contain the constitutively expressed α subunits that interact with several regulatory complexes (i.e., PA28 and PA700). The two inner rings contain the β subunits. Three of the β subunits (β1, β2, and β5) contain the catalytic sites that perform distinct proteolytic activities referred to as caspase-like (β1), trypsin-like (β2), and chymotrypsin-like (β5). These catalytic subunits form the core of the standard proteasome. In nascent proteasomes, the standard subunits can be replaced by LMP2 (β1i), MECL-1 (β2i), and LMP7 (β5i) to form the core of the immunoproteasome. A third type of catalytic core, referred to as the intermediate-type proteasome, contains a mixture of both standard and immunoproteasome catalytic subunits.[3,4]

While the standard proteasome is the predominant core particle in most tissues, immunoproteasome subunits are the major proteasome species found in tissues and cells of the immune system.[5] However, immunoproteasome subunits are also found in limited abundance in cells outside the immune system, including neurons (photoreceptors and Purkinje cells) and glia (Müller cells and astrocytes) of the retina and brain.[6–8] A recent focus of our laboratory[7,9–12] and others[6,8,13,14] has been to define conditions that provoke the upregulation of the immunoproteasome in the central nervous system. Data derived from this experimental approach provide some indication that the function of the immunoproteasome goes beyond their well-defined role in immune surveillance.[15,16] For example, the immunoproteasome is upregulated in the central nervous system in response to acute injury, disease, and age, suggesting a role in responding to stress and injury.[6–12,14,17] In addition, immunoproteasome expression in the noninjured retina and brain[6–10,12,14] and its recent localization to synapses in the brain[17] and the outer plexiform layer (OPL) in the retina[7] implies a role in normal neuronal function.

In the present study, we used immunoproteasome knockout (KO) mice missing one (*lmp7*$^{-/-}$, L7) or two (*lmp7*$^{-/-}$*/mecl-1*$^{-/-}$, L7M1) immunoproteasome subunits to test the hypothesis that the immunoproteasome is necessary to maintain normal retinal function. We found that while immunoproteasome deficiency had only minor effects on overall retinal morphology, a significant defect in retinal function, as measured by electroretinography (ERG), was observed.

Materials and Methods

Animals

C57BL/6 wild-type (WT) mice were either purchased from the National Institute on Aging–maintained colony (Harlan Sprague-Dawley, Indianapolis, IN) or were produced in our colony. Breeders for mice deficient in one (L7) or two (L7M1) catalytic subunits of the immunoproteasome were generously donated by John J. Monaco (University of Cincinnati, OH). Descriptions of gene deletions and mouse characteristics have been published.[18–20] All mice were on the C57BL/6 genetic background. The mice were housed in an animal facility maintained at

From the [1]Department of Ophthalmology, the [2]Graduate Program in the Department of Biochemistry, Molecular Biology, and Biophysics, and the [3]Histology Core for Vision Research, University of Minnesota, Minneapolis, Minnesota; the [4]Rehabilitation Research and Development Center, Atlanta VA Medical Center, Decatur, Georgia; and the [5]Department of Ophthalmology, Emory University, Atlanta, Georgia.

Supported by Grants EY013623, AG032391 (DAF), T32-AG029796 (SH), P30EY11374 (HR) from the National Institutes of Health, an unrestricted grant from Research to Prevent Blindness, and the Minnesota Lions Clubs.

Submitted for publication June 10, 2010; revised August 30, 2010; accepted September 1, 2010.

Disclosure: **S.A. Hussong**, None; **H. Roehrich**, None; **R.J. Kapphahn**, None; **M. Maldonado**, None; **M.T. Pardue**, None; **D.A. Ferrington**, None

Corresponding author: Deborah A. Ferrington, University of Minnesota, 380 Lions Research Building, 2001 6th Street SE, Minneapolis, MN 55455; ferri013@umn.edu.

20°C with a 12-hour light and dark cycle. Mice at 2, 9, 15, 20, and 24 months of age were used for the aging analysis. For the remaining studies, only 2-month-old animals were assessed. Mice were handled according to the guidelines of the Institutional Animal Care and Use Committee of the University of Minnesota and the National Institutes of Health. Animal procedures conformed to the ARVO Statement for the Use of Animals in Ophthalmic and Vision Research. The animals were killed with CO_2 and perfused with phosphate-buffered saline (PBS) with 2 U/mL heparin before tissue collection.

Retinal Protein Processing

Retinas were processed as previously described,[7,10–12,21] in a homogenization buffer containing 20 mM Tris (pH 7.4), 20% wt/vol sucrose, 2 mM $MgCl_2$, 10 mM glucose, and 2% wt/vol 3-[(3-cholamidopropyl) dimethylamino]-1-propanesulfonate (CHAPS). The supernatant containing the soluble retinal proteins from the final processing step was saved and stored at −80°C. Protein concentrations were determined with the bicinchoninic acid (BCA) assay (Pierce, Rockford, IL), with bovine serum albumin as the standard.

Western and Slot Blot Immunoassays

Western blot analysis was performed as previously described.[7,10,11,21] Slot blot immunoassays were executed on a microfiltration apparatus (Bio-Dot SF; Bio-Rad, Hercules, CA) and a 0.2-μm polyvinylidene fluoride membrane (Millipore, Billerica, MA).[21] Membranes were incubated with a primary antibody (Table 1) for 14 to 16 hours at 4°C. The appropriate secondary antibody conjugated to horseradish peroxidase (HRP; Pierce, Rockford, IL) was applied to the membrane. Reactions were developed with chemiluminescence (SuperSignal West Dura Extended Duration substrate; Pierce, Rockford, IL). Images were taken with a gel documentation system (ChemiDoc XRS; Bio-Rad), and densitometry was performed (Quantity One; Bio-Rad). The samples were normalized to a standard retina preparation run on each blot. For slot immunoblots, background was subtracted by using a buffer-only sample.

Histology and Immunohistochemistry on Retinal Sections

For all histologic analysis, tissue was fixed in 10% buffered formalin (Fischer Scientific, Pittsburgh, PA) and embedded in paraffin. Retinal sections (6 μm) were taken through the optic nerve. Before staining, the retinal sections were deparaffinized through a graded series of xylene and ethanol. For retinal morphometry measures and counts, the sections were stained with hematoxylin and eosin (H&E). Terminal deoxynucleotidyl transferase-mediated dUTP nick-end labeling (TUNEL) was performed with a kit to detect apoptosis (In Situ Cell Death Detection Kit, Fluorescein; Roche, Indianapolis, IN). For antibody staining, the tissue sections were rehydrated and then submitted to antigen retrieval by heating in 10 mM sodium citrate, 0.05% Tween 20 (pH 6.0) for 24 minutes at 94°C. Sections were blocked for 30 minutes in 10% normal donkey serum and then incubated in the primary antibodies overnight (Table 1). The reaction was visualized by using appropriate secondary antibodies. To confirm the specificity of the primary antibody, we incubated the sections in the absence of the primary antibody, with the secondary antibody alone. TUNEL-labeled and antibody-stained slides were coverslipped with antifade mounting medium containing 4′,6-diamidino-2-phenylindole (DAPI; Vectashield; Vector Laboratories, Burlingame, CA).

Retinal Morphology Measurements

The photoreceptor lengths and outer nuclear layer (ONL) and inner nuclear layer (INL) nucleus densities were measured in H&E-stained sections. Bipolar cell densities were determined from the dual staining of retinal sections with ceh-10 homeo domain containing homolog (Chx10; all bipolar cells) and protein kinase C, alpha (PKCα) (rod bipolar cells only) antibodies followed by DAPI staining of nuclei.[22] Nucleus densities and photoreceptor lengths were measured at 500 and 1000 μm on either side of the optic nerve. ONL, INL, and bipolar cell densities were determined by counting the nuclei of a specified area and dividing by the length of the measured region. Photoreceptor length was measured from the retinal pigment epithelium (RPE) to the edge of the ONL. Measurements were performed with image-analysis software (Bioquant Nova Prime, ver. 6.90.10; Bioquant Image Analysis, Nashville, TN).

The number of apoptotic nuclei was determined from counting the entire number of TUNEL-positive nuclei in the ONL of retinal sections dually stained with TUNEL and DAPI. The averaged count from four sections was used for each mouse, and the data are reported as the number of TUNEL-positive nuclei in the ONL per retinal section.

Electroretinograms

Electroretinography (ERG) was performed as described by Phillips et al.[23] Two-month-old mice were dark-adapted overnight, and ERGs were recorded with an electrophysiology system with the accompanying software (Espion^2; Espion ver. 4.0.51 software; Diagnosys LLC, Lowell, MA). Mice were anesthetized with ketamine (80 mg/kg) and xylazine (16 mg/kg). The cornea was subsequently anesthetized (0.5% tetracaine) and the pupils were dilated (1% tropicamide; 2% cyclopentolate). Body temperature was regulated with an animal temperature controller (model ATC1000; World Precision Instruments, Sarasota, FL). The active electrode was a silver DTL fiber that contacted the cornea through a layer of 0.5% carboxymethylcellulose. Subdermal needle electrodes (Grass Technologies, West Warwick, RI) were placed in the cheek and tail to serve as the reference and the ground, respectively. A Ganzfeld (ColorBurst; Espion) supported by a ring stand was positioned directly over the animal's head and produced a series of light flashes ranging from −3.3 to 1.7 log cd s/m^2. Dark-adapted ERG recordings were averaged from 3 to 10 separate light flashes at each of the 10 intensities. The interstimulus time increased from 4 to 65 seconds with increasing light flash intensity. The mice were light-adapted for 10 minutes with a background light of 1.4 log cd/m^2. Isolated cone responses were recorded with a seven-step intensity

Table 1. Antibodies Used in Immunoblot and Immunohistochemical Analyses

Antibody	Type*	Assay†	Dilution	Manufacturer
Rhodopsin	M	B	1:1000	Biodesign International, Saco, ME
Opsin: red/green	C	B	1:500	Millipore, Billerica, MA
PKCα	R_M	I	1:1000	Abcam, Cambridge, MA
Chx10	S	I	1:200	Abcam
PSD95	R_P	B	1:1000	Cell Signaling Technology, Danvers, MA
Synaptophysin	M	B	1:1000	Millipore
mGluR6	R_P	B	1:1000	Neuromics, Edina, MN
TRPM1	R_P	B	1:1000	Abcam

* M, monoclonal, host species mouse; R_M, IgG monoclonal, host species rabbit; R_P, IgG polyclonal, host species rabbit; C, IgG polyclonal, host species chicken; S, IgY polyclonal, host species sheep, IgG.

† I, immunohistochemistry; B, Western or slot blot immunoassay.

series (−0.3 to +1.7 log cd s/m^2) presented at 4 Hz with a constant background light of 1.4 log cd/m^2. Light-adapted ERGs were averaged over 25 separate light flashes for each intensity. When ERG recordings were completed, the mice were either immediately killed by CO_2 inhalation or were treated with 2 mg/kg yohimbine to reverse the effects of the xylazine and prevent corneal lesions.[24]

Electroretinogram Data Analysis

ERG a-wave amplitudes were measured from the baseline to the first negative peak. The a-wave amplitude was also measured at 7 ms for the four brightest flash intensities, to avoid any effect of b-wave changes in the summed response.[25] The b-wave amplitude was determined by measuring from the trough of the a-wave to the peak of the first positive wave. When the a-wave was absent, the b-wave was measured from the baseline to the first positive peak. The implicit time was measured from the incidence of the flash to the leading edge of the a- and b-wave peaks, respectively.

To determine the isolated photoreceptor contribution (PIII), the dark-adapted waveform data were fitted to the Hood and Birch formulation of the Lamb and Pugh model of rod phototransduction activation to determine the PIII contribution.[26] In this model, R_{mP3} is the maximum saturated photoreceptor response and is proportional to the number of ion channels in the outer segments (OS) that close in response to light, and S is the rod photoreceptor sensitivity to light.

The postreceptoral b-wave response was modeled to examine the response of the rod bipolar cells. Data from the dark-adapted b-wave was used in conjunction with the Naka-Rushton equation, to measure the maximum scotopic b-wave response (V_m) and postreceptoral sensitivity (log σ).[26]

The oscillatory potentials (OPs) were isolated from the waveform by digitally filtering signals with a band-pass of 65 to 235 Hz.[27] Each OP amplitude was measured from the peak to the trough immediately preceding it. The implicit time was measured in milliseconds from the incidence of the flash to peak of each OP. The individual OPs displayed a similar pattern so the summed OP amplitudes and implicit times were calculated from OPs 1 to 6.

Statistical Analysis

Statistical analysis for ERG a-wave, b-wave, summed OP amplitudes, and summed implicit times was performed across flash intensities and between mouse strains by repeated-measures ANOVA tests with a Greenhouse-Geisser correction (SPSS, Chicago, IL). For all other experiments, data were analyzed (NCSS 2001, Kaysville, UT). Differences between three or more groups were tested as two-way, one-way, or repeated-measures ANOVA, as indicated. When the two-way ANOVA showed significant interaction (SxA), one-way ANOVA tests were performed for each age and each strain. When appropriate, a Tukey-Kramer post hoc test was performed. When data failed normality assumptions of the one-way ANOVA, a Kruskal-Wallis (KW) one-way ANOVA on ranks was performed, followed by a z-value multiple-comparisons test. Significance was set at $P < 0.05$ for all statistical measures.

Results

Altered Retinal Morphology with Aging and Immunoproteasome Deficiency

Comparison of H&E-stained retinal sections from 2-month-old mice showed that the overall retinal morphology was essentially the same across strains (Fig. 1A). To quantitatively assess whether retinal morphology is altered with age or strain, we measured the density of the ONL and INL. The ONL contains the nuclei of the photoreceptors and therefore, the density of the nuclei is a measure of the relative content of photoreceptors. The density of the nuclei in the ONL decreased by 11% with age at both 500 and 1000 μm from the optic nerve (Fig. 1B). At 500 μm from the optic nerve, the number of ONL nuclei was dependent on age and strain (two-way ANOVA, $F_{(8,133)} = 2.74$, $P = 0.008$). At 1000 μm, only a significant decrease in ONL nuclei across ages was observed (two-way ANOVA, $F_{(4,133)} = 4.64$, $P = 0.002$). Thus, only minor defects in retinal morphology are evident in L7M1 mice which exhibit approximately 6% fewer nuclei in the ONL compared with WT and L7 (Fig. 1B).

To determine whether the differences in the density of nuclei in the ONL with aging and between strains were due to a loss of cells via apoptosis, retinal sections were stained with TUNEL and the number of nuclei undergoing apoptosis in the ONL was counted (Fig. 1C). (The number of apoptotic cells in the other nuclear layers of the retina was negligible [data not shown]). Overall, age- and strain-dependent decreases in nuclei in the ONL correlated with significant increases in apoptotic nuclei (two-way ANOVA, $F_{(8,124)} = 2.41$, $P = 0.02$). For all strains, the number of apoptotic nuclei was approximately twofold higher at 15 months than at 2 months. The level of apoptosis reached its peak at 20 months, when the number of apoptotic nuclei was 2.5-fold higher than in 2-month-old animals (one-way ANOVA, WT, $H_{(4)} = 16.93$, $P = 0.002$; L7, $F_{(4,27)} = 4.14$, $P < 0.01$; L7M1, $F_{(4,48)} = 15.66$, $P < 0.001$). These data are consistent with an apoptotic mechanism of cell death with aging. In addition, apoptosis levels in L7M1 ONL were, on average, 1.7-fold higher than both WT and L7 (one-way ANOVA: 2 months, $F_{(2,32)} = 7.21$, $P = 0.003$; 15 months, $H_{(2)} = 16.47$, $P < 0.001$; 20 months, $F_{(2,16)} = 9.55$, $P = 0.002$). The increased apoptosis levels correlate with the observed decrease in nuclei in the ONL. The elevated apoptosis in L7M1 retinas that was not replicated in L7 suggests that the MECL-1 subunit, which is present in the L7 and WT mice, is crucial in preventing apoptotic cell death of photoreceptors.

The density of nuclei in the INL, which contains bipolar, amacrine, and horizontal cell nuclei, decreased approximately 13% with age at both 500 μm (two-way ANOVA: $F_{(4,132)} = 9.51$, $P < 0.001$) and 1000 μm (two-way ANOVA: $F_{(4,133)} = 4.01$, $P = 0.004$) from the optic nerve (Fig. 1D). However, there were no significant differences in the density of nuclei in the INL between strains (500 μm, $P = 0.21$; 1000 μm, $P = 0.16$). The age-related loss of nuclei observed in both the ONL and INL is consistent with previously reported data in aged C57BL/6 mice.[28,29]

Decreased Retinal Function with Immunoproteasome Deficiency

To determine the effect of immunoproteasome deficiency on retinal function, we performed dark- and light-adapted ERGs on 2-month-old WT, L7, and L7M1 mice. At this age, there is no difference in retinal morphology (Fig. 1), so any change in the ERG can be attributed to the absence of specific immunoproteasome subunits rather than secondary effects associated with aging.

Comparing WT and immunoproteasome KO mice, dark-adapted ERGs from WT showed significantly larger waveforms (Fig 2A). At the two highest flash intensities, the dark-adapted a-wave amplitude, reflecting the function of the photoreceptors, was 20% lower in both L7 and L7M1 mice compared with WT (repeated measures ANOVA, $F_{(4.95,61.8)} = 3.61$, $P = 0.006$; Fig. 2B). More dramatic differences were seen in the dark-adapted b-wave amplitudes, reflecting the electrical activity of the bipolar cells. Dark-adapted b-wave amplitudes in immunoproteasome-deficient mice were 22% to 27% lower than in the WT at all flash intensities above −0.70 log cd m/s^2 ($F_{(4.25,53.17)} = 4.00$, $P = 0.006$; Fig. 2C). A plot of the relationship between a- and b-wave amplitudes further confirms that the b-wave was more dramatically altered at all intensities in the immunopro-

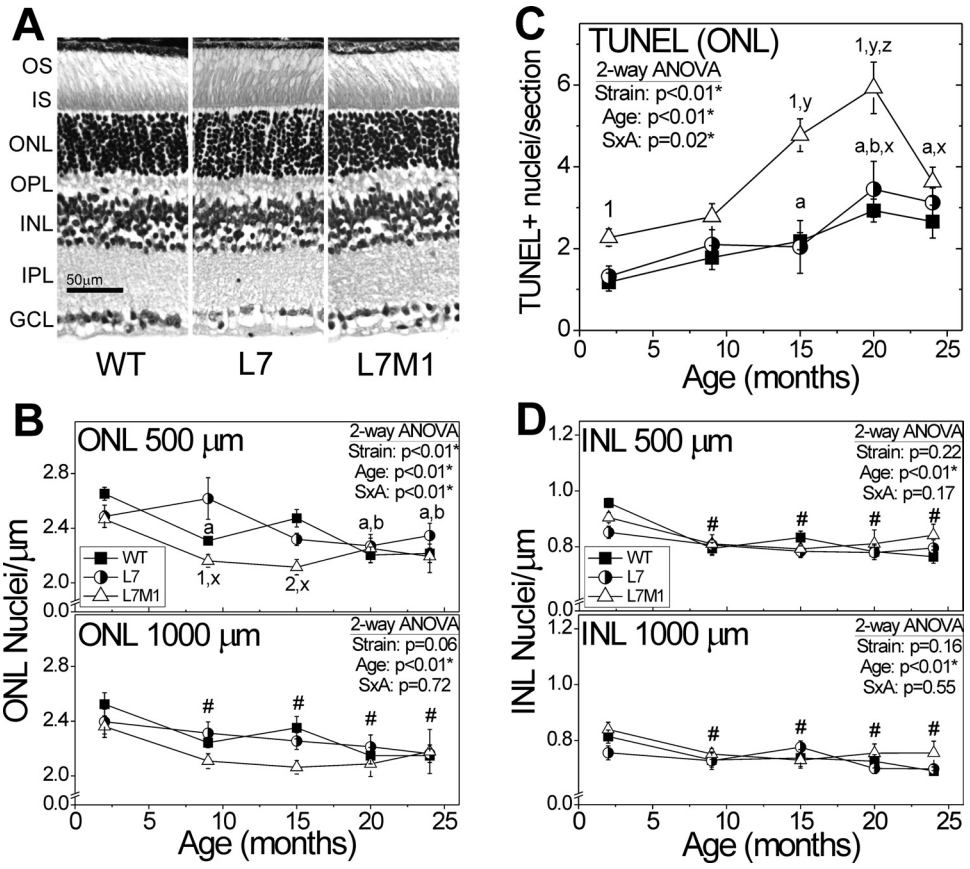

FIGURE 1. Age- and strain-related changes in retinal morphology and apoptosis. (**A**) Representative paraffin-embedded retinal sections stained with H&E from 2-month-old WT, L7, and L7M1 mice. Images were taken with a 20× objective. GCL, ganglion cell layer; OS, photoreceptor OS. (**B–D**) Summary of retinal morphology and TUNEL measurements for WT, L7, and L7M1 retinas. Two-way ANOVA results are provided in each panel. When there was significant interaction (SxA), one-way ANOVA comparisons were performed for each strain and each age. Results of Tukey-Kramer post hoc comparisons are indicated by letters, numbers, or symbols. (**B**) ONL nuclei counted at 500 and 1000 μm from the optic nerve. Two-way ANOVA for the density of nuclei at 500 μm showed significant interaction ($F_{(8,133)} = 2.74$, $P < 0.01$). One-way ANOVA results by strain with age (WT, $P < 0.001$; L7M1, $P = 0.001$): a, different from WT at 2 months; b, different from WT at 15 months; and x, different from L7M1 at 2 months. One-way ANOVA results by age between strains: (9 months, $P = 0.008$, 15 months, $P < 0.001$): 1, different from L7 and WT at 9 months; and 2, different from WT at 15 months. Two-way ANOVA for the density of nuclei at 1000 μm showed a significant decline with age ($F_{(4,133)} = 4.64$, $P = 0.002$); #different from 2 months. (**C**) TUNEL-positive nuclei in the ONL. Two-way ANOVA for TUNEL positive nuclei in the ONL showed significant interaction ($F_{(8,124)} = 2.41$, $P = 0.02$). One-way ANOVA results by strain with age (WT, $P = 0.002$; L7, $P < 0.01$; L7M1 $P < 0.001$): a, different from WT 2 months; b, different from WT 9 months; x, different from L7 2 months; y, different from L7M1 2 and 9 months; and z, different from L7M1 24 months. One-way ANOVA results by age between strains: (2 months, $P = 0.003$; 15 months, $P < 0.001$; 20 months, $P = 0.002$) 1, different from L7 and WT. (**D**) Counts of INL nuclei decreased with age at both 500 μm (two-way ANOVA $F_{(4,132)} = 9.51$, $P < 0.001$) and 1000 μm (two-way ANOVA $F_{(4,133)} = 4.01$, $P = 0.004$) from the optic nerve; #different from 2 months. However there were no differences between strains at either 500 μm ($P = 0.21$) or 1000 μm ($P = 0.16$). Data are shown as the mean ± SEM. WT n = 7–18; L7 n = 5–11; and L7M1 n = 6–19 per group.

teasome-deficient retinas (Fig. 2D). Defects in the a-wave are observed only at the highest intensities.

Cone-mediated, light-adapted b-wave amplitudes were also significantly higher in WT than in immunoproteasome-deficient retinas (Fig. 3A). L7 amplitudes plotted across flash intensities showed that the response was 19% to 34% lower than that in both the WT and L7M1 at flash intensities greater than or equal to 0.35 log cd m/s^2 ($F_{(4.22,52.8)} = 6.56$, $P < 0.001$; Fig. 3B). L7M1 light-adapted b-wave amplitudes were significantly lower (11% and 16%, respectively) than those of the WT at the two brightest flash intensities ($P < 0.001$; 1.30 and 1.70 log cd m/s^2).

The implicit times for the dark-adapted a- and b-wave and light-adapted b-wave were also evaluated to determine whether immunoproteasome deficiency has an effect on the response rate after a light stimulus. There was no significant difference between strains in either the dark-adapted a-wave ($P = 0.09$) or light-adapted b-wave ($P = 0.86$) implicit times (Figs. 4A, 4C). Notably, the dark-adapted b-wave response was significantly faster in both immunoproteasome KO strains ($F_{(2,25)} = 4.30$, $P = 0.03$; Fig. 4B).

The decrease in the dark-adapted b-wave implicit time could lead to a premature truncation of the a-wave.[25] To determine whether the decrease in the dark-adapted a-wave could be an artifact of a faster b-wave, we reanalyzed the a-wave amplitude at 7 ms at the four highest flash intensities in all strains. This time point occurs before the first negative peak in all ERG waveforms. At 7 ms, the dark-adapted a-wave amplitudes were not significantly different between the WT and the KO mice ($P = 0.45$), suggesting no difference in photoreceptor response to light (Fig. 2E).

To confirm the results of the raw waveform analysis, we also evaluated the isolated components of the ERG measurements by fitting the waveform data to models as described in the Methods section. The isolated scotopic photoreceptor contribution (PIII) provides the maximum photoreceptor response (R_{mP3}), which is proportional to the number of ion channels in the rod OS that close in the response to light and the retinal photoreceptor sensitivity to light (S) (Fig. 5A). When the ERG waveforms were fit to this model, there was a 35% decrease in the maximum rod photoreceptor response (R_{mP3}) in both L7 and L7M1 mice. However, because of the high variability between animals, this apparent difference between strains was not significant ($P = 0.058$). There was no difference in retinal sensitivity (S) between strains ($P = 0.38$). These data agree with the dark-adapted a-wave analyzed at 7 ms, indicating that there was no change in the photoreceptor response in L7 and L7M1 mice.

The postreceptoral b-wave response was modeled to measure the maximum scotopic b-wave response (V_{mDA}) and the postreceptoral sensitivity (log σ). The sensitivity of the postreceptoral response was not significantly different in log σ ($P = 0.86$; Fig. 5B). The L7 and L7M1 mice exhibited a 30% decrease in the maximum dark-adapted b-wave (V_{mDA}; $H_{(2)} = 12.90$,

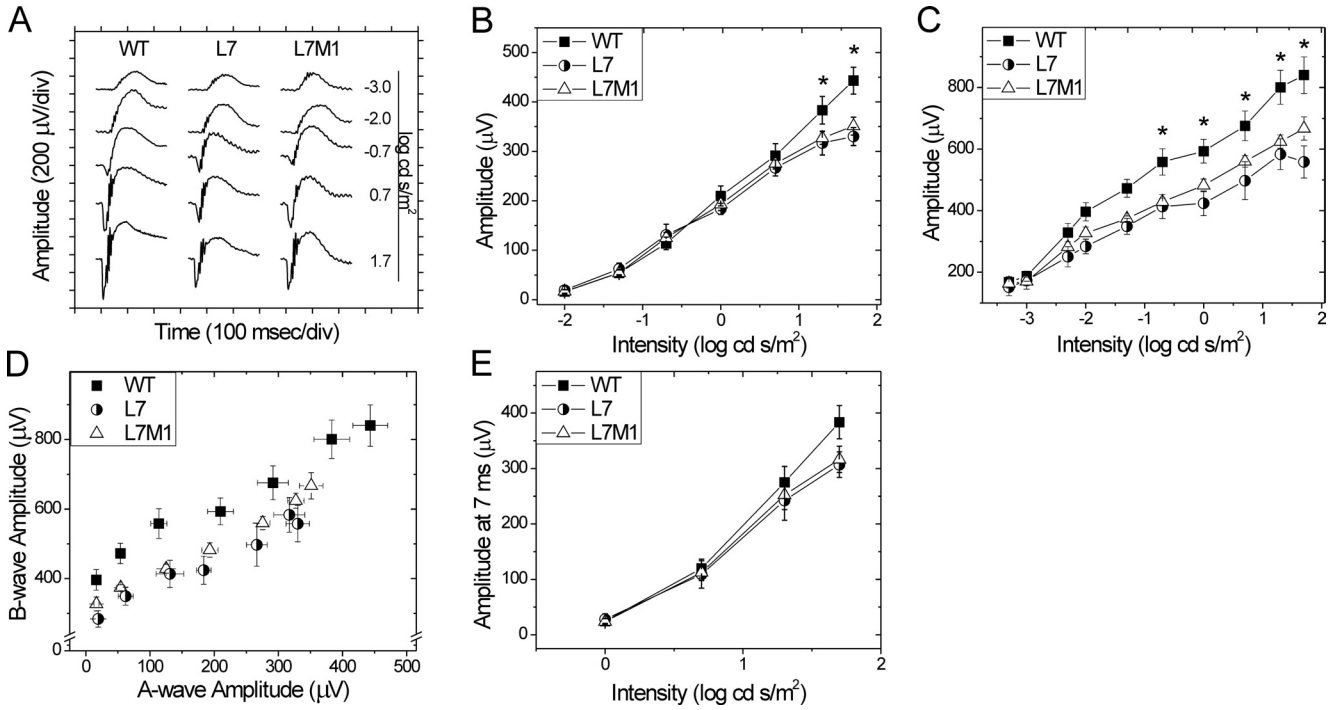

FIGURE 2. Strain-related changes in dark-adapted retinal response measured by electroretinography. (**A**) Representative dark-adapted waveforms for 2-month-old WT, L7, and L7M1 mice. (**B–D**) Average dark-adapted amplitudes from ERGs performed on WT, L7, and L7M1 mice. (**B**, **C**) Repeated-measures ANOVA tests were performed: *WT different from L7M1 and L7. (**B**) Dark-adapted a-wave amplitudes ($F_{(4.95,61.8)} = 3.61$, $P = 0.006$). (**C**) Dark-adapted b-wave amplitudes ($F_{(4.25,53.17)} = 4.00$, $P = 0.006$). (**D**) Dark-adapted b-wave plotted against the dark-adapted a-wave. (**E**) Dark-adapted a-wave amplitude at 7 ms ($P = 0.45$). WT $n = 11–12$; L7 $n = 6$; and L7M1 $n = 10$.

$P = 0.002$) compared with WT (Fig. 5B). These data are consistent with the raw b-wave amplitude measures indicating a significant difference in the bipolar cell response of the immunoproteasome-deficient retinas.

The effects of immunoproteasome deficiency on OP amplitude and implicit time were also examined. The individual OPs displayed a similar pattern between strains, and so the summed OP amplitudes and implicit times were analyzed. No significant difference in summed OP amplitudes ($P = 0.42$) or implicit times ($P = 0.06$) was observed between strains (Fig. 6).

Assessment of Cells and Proteins Involved in the ERG Response

To begin exploring the potential mechanisms responsible for the loss in retinal function exhibited by KO mice, we quantified the cells specifically involved in producing the ERG signal (i.e., photoreceptor and bipolar cells) as well as the levels of select proteins involved in visual transmission. The relative levels of photoreceptor proteins (rhodopsin [rods] and opsin [cones]) was determined using slot blot immunoassays. In 2-month-old mice, no difference in rhodopsin ($P = 0.99$) or opsin ($P = 0.63$) content was observed between the strains (Fig. 7A). Consistent with these results, no difference in photoreceptor OS length (measured on H&E-stained retinal sections) was observed comparing immunoproteasome-deficient with WT retinas ($P = 0.26$; data not shown).

The b-wave response is mainly produced from the bipolar cells whose nuclei are located in the INL. Retinal morphology data did not show a difference in the density of nuclei in the INL between mouse strains (Fig. 1C). However, the INL contains nuclei of multiple cell types (i.e., amacrine, horizontal, and bipolar cells) and thus counts of nuclei are not specific for bipolar cells.[30] To determine whether there was a specific loss in rod or cone bipolar cells, we performed counts of total bipolar and rod-specific bipolar cells in retinal sections double-stained with antibodies to Chx10 (bipolar cell marker) and PKCα (rod bipolar cell marker). Rod bipolar cells were identified by the colocalization of Chx10 and PKCα.[22] Conversely, cone bipolar cells stained with Chx10 only. No significant difference in either total ($P = 0.67$) or rod ($P = 0.33$) bipolar cell density was observed between the strains (Fig. 8). Therefore, changes in the number of total or photoreceptor-specific bipolar cells does not account for the observed decrease in bipolar cell response in L7 and L7M1 mice.

Although the overall counts of the cell types that produce the ERG signal are not changed with immunoproteasome deficiency, the proteins involved in transmitting the visual signal could be affected. The proteasome is a key regulator of the protein levels of some of the synaptic proteins, such as PSD95, synaptophysin, and several glutamate receptors.[31,32] It is plausible that the immunoproteasome regulates the levels of a subset of these proteins. To determine whether immunoproteasome deficiency affects synaptic protein levels, we examined the presynaptic protein PSD95 (postsynaptic density protein 95), the synaptic vesicle protein synaptophysin and the postsynaptic proteins metabotropic glutamate receptor 6 (mGluR6) and transient receptor potential member 1 (TRPM1) by Western blot. There was no significant difference in the content of either PSD95 ($P = 0.44$) or synaptophysin ($P = 0.51$; Fig. 7B). As a caveat, it is important to mention that both PSD95 and synaptophysin are located both in the IPL and OPL, which could reduce the sensitivity of this assay in detecting changes localized to the OPL.[33,34]

TRPM1 is a bipolar cell protein that was recently identified as the cation channel that generates the b-wave.[35,36] The 184-kDa isoform makes the cation channel but the function of the other isoforms remains unclear.[36] There was no difference in

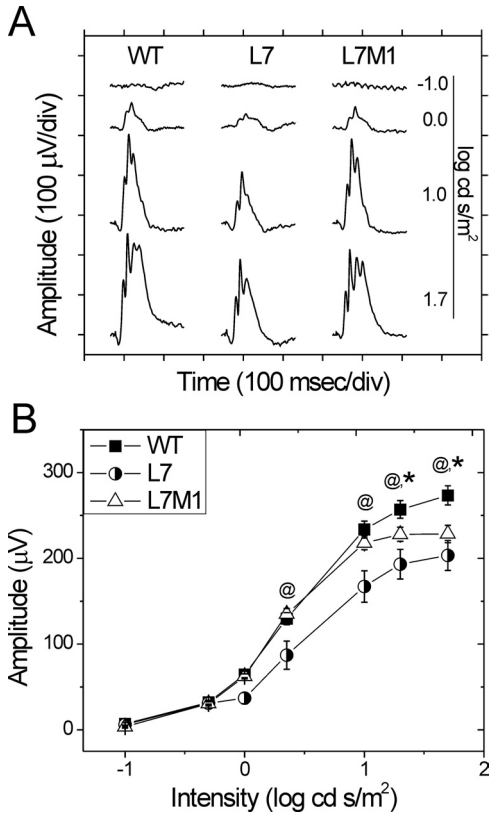

FIGURE 3. Strain-related changes in light-adapted retinal response measured by electroretinography. (**A**) Representative light-adapted waveforms for 2-month-old WT, L7, and L7M1 mice. (**B**) Average light-adapted b-wave amplitudes from ERGs performed on WT, L7, and L7M1 mice. Repeated measures ANOVA tests were performed: *WT different from L7M1 and L7; @, L7 different from WT and L7M1. L7 and L7M1 KO mice had significantly lower amplitudes than the WT ($F_{(4.22,52.8)} = 6.56$, $P < 0.001$). Data are shown as the mean ± SEM. WT $n = 12$; L7 $n = 6$; L7M1 $n = 10$.

the protein content of any of the TRPM1 isoforms, including the 184-kDa cation channel ($P \geq 0.11$; Fig. 7C).

The bipolar cell glutamate receptor mGluR6 is the initiator of the G-protein cascade that ultimately opens the TRPM1 cation channel. There was an approximate 30% decrease in mGluR6 in L7 and L7M1 retinas compared with WT. Because of the large variability in the sample group, a nonparametric test was used, and therefore the decrease was not significant. ($P = 0.13$; Fig. 7B).

DISCUSSION

In the present study, we used immunoproteasome KO mice lacking either one (L7) or two (L7M1) catalytic subunits of the immunoproteasome to test the hypothesis that the immunoproteasome is essential for the maintenance of normal retinal function. Retinal morphometry (Fig. 1) and quantitative measures of several retinal cell types (photoreceptor and bipolar cells; Fig. 7, 8) showed no major abnormalities in overall retinal morphology in KO mice. Evaluation of retinal function by ERG showed significantly decreased amplitude in the dark- and light-adapted b-waves, suggesting that immunoproteasome deficiency is associated with both rod and cone pathway defects (Figs. 2–4). Correlation plots of a- and b-wave amplitudes (Fig. 2) and altered implicit times (Fig. 4) further imply abnormal signal transmission resulting from defects in the secondary neurons. Analysis of the levels of a subset of proteins involved in signal transmission showed no significant decrease. Taken together, the data suggest that immunoproteasome deficiency causes defects in bipolar cell response. These results support a previously unrecognized role for the immunoproteasome in vision transduction.

The immunoproteasome has a well-described role in the immune system. Therefore, it is possible that the loss in retinal function observed in L7 and L7M1 mice could be due to changes in the systemic immune system that could affect overall retinal health. Based on the literature, there is no evidence that these mice are immunologically impaired (i.e., develop autoimmune disease or immunodeficiency). In fact, only minor

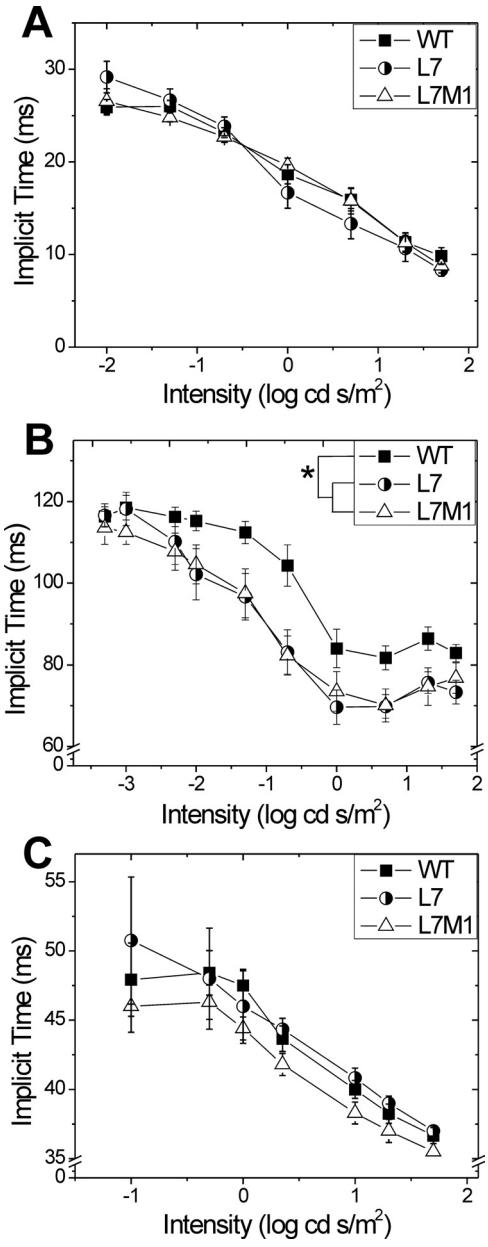

FIGURE 4. Strain-related changes in ERG implicit time. (**A**–**C**) Average implicit times from ERGs performed on WT, L7, and L7M1 mice. Repeated-measures ANOVA tests were performed. (**A**) Dark-adapted a-wave implicit times ($P = 0.09$). (**B**) Dark-adapted b-wave implicit times. Repeated-measures ANOVA revealed a strain effect: ($F_{(2,25)} = 4.30$, $P = 0.03$) *different from WT. (**C**) Light-adapted b-wave implicit times ($P = 0.86$). Data are shown as mean ± SEM. WT $n = 12$; L7 $n = 6$; L7M1 $n = 10$.

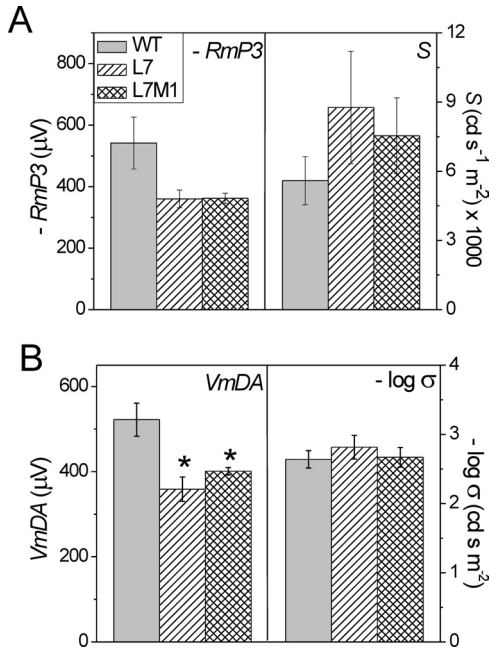

FIGURE 5. Strain-related changes in ERG parameters. Average ERG parameters derived from mathematical models from WT, L7, and L7M1 mice. One-way ANOVA or KW one-way ANOVA followed by Tukey-Kramer or *z*-value multiple-comparison tests were performed; *different from WT at $P < 0.05$. (**A**) Isolated rod photoreceptor response (R_{mP3}; $P = 0.058$) and sensitivity (S; $P = 0.38$) of WT, L7, and L7M1 retinas. (**B**) Maximum dark-adapted postreceptoral response (bipolar cells) (V_{mDA}; $H_{(2)} = 12.90$, $P = 0.002$) and sensitivity (log σ; $P = 0.86$). Data are shown as the mean ± SEM. WT $n = 11$; L7 $n = 6$; L7M1 $n = 9$.

changes in T-cell populations and proliferation in L7 and L7M1 mice have been reported.[19,20] Under our laboratory conditions, the mice are healthy and breed successfully. In addition, there is no evidence of retinal inflammation based on the lack of gross morphologic changes up to 24 months of age (Fig. 1). Overall, there is currently no evidence that the lack of specific immunoproteasome subunits can substantially impair the systemic immune function. However, subtle, currently undescribed changes in the immune system that have an effect on retinal function are possible.

Another potential mechanism behind the altered ERG waveforms in immunoproteasome KO mice could be that the content of some proteins involved in phototransduction or visual transmission are regulated by the immunoproteasome. The direct knockout of many of these visual transmission proteins (i.e., RPE65, rhodopsin, TRPM1, and mGluR6) causes a severe ERG phenotype (greater than a 75% decrease in amplitudes).[29,35,37–43] In immunoproteasome KO mice, we observed only a 25% decrease in the dark-adapted b-wave. In the present study, we evaluated the levels of select proteins in each pathway and found a 30% decrease in mGluR6 in the KO mice. Although this change was not significant, it suggests there could be subtle changes in the levels of other proteins as well. The synergistic effect of altering the expression of several proteins involved in visual transmission could have an effect on retinal function. Ongoing comparative analysis of the retinal proteome will provide important molecular details of how immunoproteasome deficiency affects the retina.

In addition to the proteins directly involved in signal transduction or transmission, changes in proteins required for maintaining retinal structural integrity can also cause altered ERG waveforms. Mutations or elimination of the structural proteins bassoon, dystroglycan, and retinoschisin results in a decrease in the b-wave that has been associated with the inability to efficiently transmit the visual signal from the photoreceptors to the bipolar cells.[44–46] The gross retinal morphology of bassoon and dystroglycan mutants both appear normal; however, ultrastructural changes in ion channels or synaptic spherules are present.[44,45] An in-depth investigation of synaptic junction morphology of immunoproteasome KO retinas could help determine whether subtle changes in alignment of synapses between photoreceptors and bipolar cells is responsible for their decreased visual transmission.

Altered ERG waveforms have also been observed with reduction or elimination of proteins that are not directly linked to vision but that are ubiquitously involved in maintaining retinal homeostasis. One of the critical requirements for maintaining retinal homeostasis is the tight regulation of cellular redox status, which reflects the balance between production and elimination of harmful reactive oxygen and nitrogen species. These reactive molecules can perturb homeostasis by damaging DNA, lipids, and proteins. In the retina, the highly abundant copper-zinc superoxide dismutase (CuZn SOD) is a key antioxidant for maintaining retinal homeostasis via elimination of superoxide.[47] Recent studies of retinal function in CuZn SOD KO mice (*sod1*$^{-/-}$) showed ~30% reduction in both a- and b-wave amplitudes that correlated with a 15% to 20% decrease in the density of nuclei in the ONL and INL.[48] In addition, ribozyme-induced reduction of the manganese SOD (MnSOD; *sod2*), which is localized to the mitochondria, also caused a similar reduction in a- and b-wave amplitudes and ONL nuclei.[49] Conversely, the neuroprotective effect of boost-

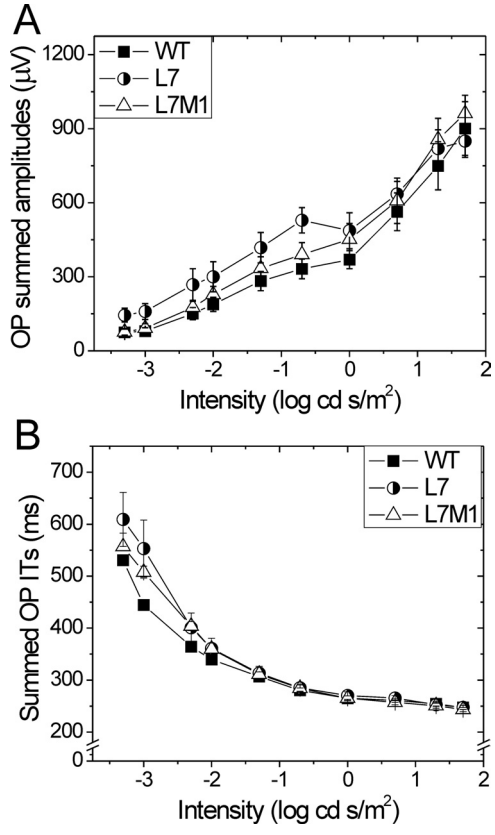

FIGURE 6. Summary of filtered oscillatory potentials. (**A**) Summed amplitudes of oscillatory potentials 1 to 6 from WT, L7, and L7M1 mice. Repeated-measures ANOVA showed no significant difference between strains ($P = 0.42$). (**B**) Summed implicit times (ITs) for oscillatory potentials 1 to 6. Repeated-measures ANOVA showed no significant difference between strains ($P = 0.06$). Data are shown as mean ± SEM. WT $n = 11$; L7 $n = 6$; L7M1 $n = 9$.

ing cellular antioxidant capacity via induced expression of antioxidant enzymes or the introduction of antioxidant supplements in various retinal degeneration models suggests a critical role for tight regulation of redox status in retinal function.[50–52]

In our previous work, we have shown that retinal cells respond to elevated levels of oxidative stress due to disease,[9] aging,[10] and exposure of cultured cells to peroxide[10] by upregulating the immunoproteasome. These results imply an important role for the immunoproteasome in responding to and protecting against oxidative damage. Consistent with this idea, retinal pigment epithelial cells from L7M1 mice were more susceptible to peroxide-induced death than WT cells.[10] There are several possible means by which the immunoproteasome protects cells from oxidative damage. As has been suggested previously, the immunoproteasome could be involved in the degradation of oxidatively modified proteins.[53] Inadequate turnover of damaged proteins caused by immunoproteasome deficiency could allow dysfunctional proteins involved in visual transmission to accumulate. The immunoproteasome could also participate in cell signaling in response to oxidative stress by regulating the content of key proteins in the cascade. Activation of the kinase Akt[54] and transcription factor NFκB[55,56] are two examples where the immunoproteasome has been linked to the regulation of stress-induced signaling.

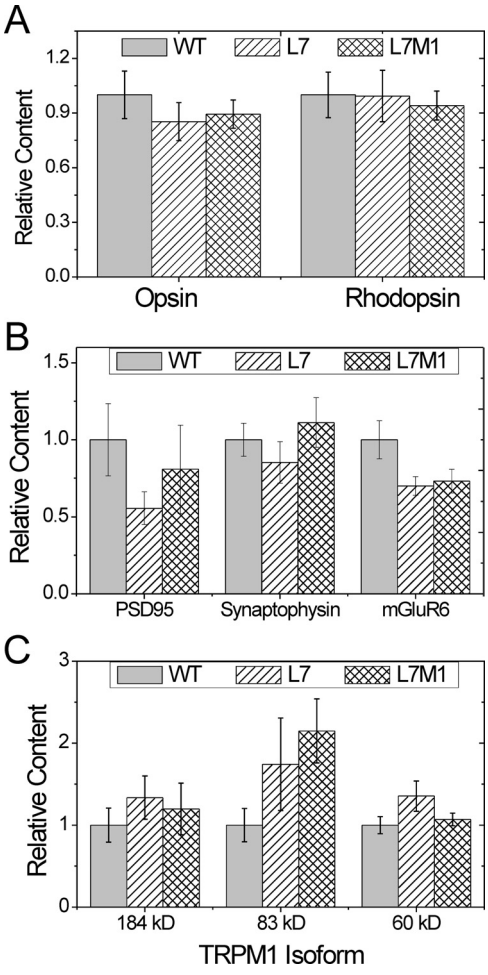

Figure 7. Content of photoreceptor and synaptic proteins. Summary immunoblot data for retinal photoreceptor and synaptic proteins from two-month-old WT, L7, and L7M1 mice. One-way ANOVA or KW one-way ANOVA was performed for each protein. (**A**) Relative content measured from slot immunoblots for photoreceptor proteins: rhodopsin and opsin. There were no significant differences between strains in either relative opsin ($P = 0.63$) or rhodopsin ($P = 0.99$) content. (**B**) Relative Western blot density for synaptic proteins: PSD95, synaptophysin, and mGluR6. There was no significant difference between strains for PSD95 ($P = 0.44$), synaptophysin ($P = 0.51$) or mGluR6 ($P = 0.14$). (**C**) Relative Western blot density for three TRPM1 isoforms: 184, 83, and 60 kDa. ANOVA showed no significant difference between strains for any isoform ($P = 0.56$; $P = 0.11$; $P = 0.18$, respectively). Data are shown as the mean ± SEM. WT $n = 6$–19; L7 $n = 4$–18; and L7M1 $n = 6$–14 per group.

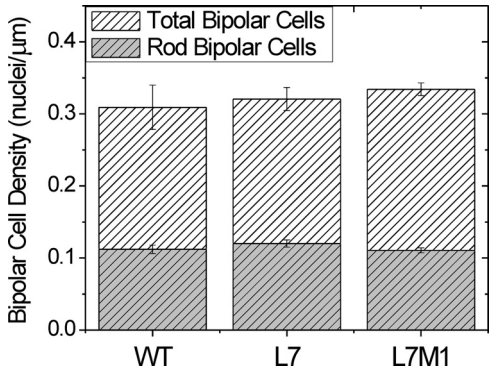

Figure 8. Unaltered bipolar cell densities in 2-month-old WT, L7, and L7M1 retina. Summary of bipolar cell densities and distribution of rod and cone bipolar cell populations. One-way ANOVA tests were performed on total and rod bipolar cell density. No significant difference was detected between strains for either total ($P = 0.67$) or rod ($P = 0.33$) bipolar cell density. Data are shown as the mean ± SEM. WT $n = 5$; L7 $n = 6$; and L7M1 $n = 6$.

The proteasome degrades protein substrates into peptides ranging in size from 3 to 22 amino acids.[57] Some of these peptides could be biologically active and regulate proteins or pathways critical for normal vision transmission. The importance of neuropeptides and hormones generated by carboxypeptidase E in maintaining normal vision transmission was demonstrated in carboxypeptidase E KO mice, which exhibit decreased b-wave amplitudes and altered synaptic vesicle biogenesis.[58,59] Previous reports have shown that the standard, intermediate-type, and immunoproteasome produce peptides that are unique to each proteasome subtype.[3,60] While WT retina most likely contains all three proteasome subtypes, L7 and L7M1 retinas (which still have the full complement of LMP2) contain only populations of standard and intermediate-type proteasome subunits.[10] Therefore, the difference in proteasome subpopulations may result in diminished ERG response in KO mice through the absence of biologically active peptides uniquely produced by the immunoproteasome.

In conclusion, using immunoproteasome-deficient mice, we have demonstrated an essential role for the immunoproteasome in normal vision transmission. These results, along with those in our previous reports suggesting a role for the immunoproteasome in responding to stress and injury,[7,10] provide unequivocal evidence that the immunoproteasome functions beyond its well-described role in immune surveillance. Thus, the name "immunoproteasome" is misleading, since it acknowledges only one aspect of the ever-increasing roles discovered for this intriguing protein.

Acknowledgments

The authors thank Dale Gregerson for thoughtful discussions.

References

1. Goldberg AL. Functions of the proteasome: the lysis at the end of the tunnel. *Science.* 1995;268:522–523.

2. Grune T, Merker K, Sandig G, Davies KJ. Selective degradation of oxidatively modified protein substrates by the proteasome. *Biochem Biophys Res Commun.* 2003;305:709–718.
3. Dahlmann B, Ruppert T, Kuehn L, Merforth S, Kloetzel PM. Different proteasome subtypes in a single tissue exhibit different enzymatic properties. *J Mol Biol.* 2000;303:643–653.
4. Klare N, Seeger M, Janek K, Jungblut PR, Dahlmann B. Intermediate-type 20 S proteasomes in HeLa cells: "asymmetric" subunit composition, diversity and adaptation. *J Mol Biol.* 2007;373:1–10.
5. Eleuteri AM, Kohanski RA, Cardozo C, Orlowski M. Bovine spleen multicatalytic proteinase complex (proteasome): replacement of X, Y, and Z subunits by LMP7, LMP2, and MECL1 and changes in properties and specificity. *J Biol Chem.* 1997;272:11824–11831.
6. Díaz-Hernández M, Hernández F, Martín-Aparicio E, et al. Neuronal induction of immunoproteasome in Huntington's disease. *J Neurosci.* 2003;23:11653–11661.
7. Ferrington DA, Hussong SA, Roehrich H, et al. Immunoproteasome responds to injury in the retina and brain. *J Neurochem.* 2008;106:158–169.
8. Mishto M, Bellavista E, Santoro A, et al. Immunoproteasome and LMP2 polymorphism in aged and Alzheimer's disease brains. *Neurobiol Aging.* 2006;27:54–66.
9. Ethen CM, Hussong SA, Reilly C, Feng X, Olsen TW, Ferrington DA. Transformation of the proteasome with age-related macular degeneration. *FEBS Lett.* 2007;581:885–890.
10. Hussong SA, Kapphahn RJ, Phillips SL, Maldonado M, Ferrington DA. Immunoproteasome deficiency alters retinal proteasome's response to stress. *J Neurochem.* 2010;113:1481–1490.
11. Kapphahn RJ, Bigelow EJ, Ferrington DA. Age-dependent inhibition of proteasome chymotrypsin-like activity in the retina. *Exp Eye Res.* 2007;84:646–654.
12. Louie JL, Kapphahn RJ, Ferrington DA. Proteasome function and protein oxidation in the aged retina. *Exp Eye Res.* 2002;75:271–284.
13. Ding Q, Reinacker K, Dimayuga E, et al. Role of the proteasome in protein oxidation and neural viability following low-level oxidative stress. *FEBS Lett.* 2003;546:228–232.
14. Gavilán MP, Castaño A, Torres M, et al. Age-related increase in the immunoproteasome content in rat hippocampus: molecular and functional aspects. *J Neurochem.* 2009;108:260–272.
15. Goldberg AL, Cascio P, Saric T, Rock KL. The importance of the proteasome and subsequent proteolytic steps in the generation of antigenic peptides. *Mol Immunol.* 2002;39:147–164.
16. Rock KL, Gramm C, Rothstein L, et al. Inhibitors of the proteasome block the degradation of most cell proteins and the generation of peptides presented on MHC class I molecules. *Cell.* 1994;78:761–771.
17. Nguyen TP, Soukup VM, Gelman BB. Persistent hijacking of brain proteasomes in HIV-associated dementia. *Am J Pathol.* 2010;176:893–902.
18. Basler M, Moebius J, Elenich L, Groettrup M, Monaco JJ. An altered T cell repertoire in MECL-1-deficient mice. *J Immunol.* 2006;176:6665–6672.
19. Caudill CM, Jayarapu K, Elenich L, Monaco JJ, Colbert RA, Griffin TA. T cells lacking immunoproteasome subunits MECL-1 and LMP7 hyperproliferate in response to polyclonal mitogens. *J Immunol.* 2006;176:4075–4082.
20. Fehling HJ, Swat W, Laplace C, et al. MHC class I expression in mice lacking the proteasome subunit LMP-7. *Science.* 1994;265:1234–1237.
21. Kapphahn RJ, Giwa BM, Berg KM, et al. Retinal proteins modified by 4-hydroxynonenal: identification of molecular targets. *Exp Eye Res.* 2006;83:165–175.
22. Morrow EM, Chen CM, Cepko CL. Temporal order of bipolar cell genesis in the neural retina. *Neural Dev.* 2008;3:2.
23. Phillips MJ, Walker TA, Choi HY, et al. Tauroursodeoxycholic acid preservation of photoreceptor structure and function in the rd10 mouse through postnatal day 30. *Invest Ophthalmol Vis Sci.* 2008;49:2148–2155.
24. Guillet R, Wyatt J, Baggs RB, Kellogg CK. Anesthetic-induced corneal lesions in developmentally sensitive rats. *Invest Ophthalmol Vis Sci.* 1988;29:949–954.
25. Robson JG, Saszik SM, Ahmed J, Frishman LJ. Rod and cone contributions to the a-wave of the electroretinogram of the macaque. *J Physiol.* 2003;547:509–530.
26. Akula JD, Hansen RM, Martinez-Perez ME, Fulton AB. Rod photoreceptor function predicts blood vessel abnormality in retinopathy of prematurity. *Invest Ophthalmol Vis Sci.* 2007;48:4351–4359.
27. Akula JD, Mocko JA, Moskowitz A, Hansen RM, Fulton AB. The oscillatory potentials of the dark-adapted electroretinogram in retinopathy of prematurity. *Invest Ophthalmol Vis Sci.* 2007;48:5788–5797.
28. Gresh J, Goletz P, Crouch RK, Rohrer B. Structure-function analysis of rods and cones in juvenile, adult, and aged C57BL/6 and Balb/c mice. *Vis Neurosci.* 2003;20:211–220.
29. Rohrer B, Goletz P, Znoiko S, et al. Correlation of regenerable opsin with rod ERG signal in Rpe65$^{-/-}$ mice during development and aging. *Invest Ophthalmol Vis Sci.* 2003;44:310–315.
30. Jeon CJ, Strettoi E, Masland RH. The major cell populations of the mouse retina. *J Neurosci.* 1998;18:8936–8946.
31. Colledge M, Snyder EM, Crozier RA, et al. Ubiquitination regulates PSD-95 degradation and AMPA receptor surface expression. *Neuron.* 2003;40:595–607.
32. Wheeler TC, Chin L, Li Y, Roudabush FL, Li L. Regulation of synaptophysin degradation by mammalian homologues of Seven in Absentia. *J Biol Chem.* 2002;277:10273–10282.
33. Brandstätter JH, Dick O, Boeckers TM. The postsynaptic scaffold proteins ProSAP1/Shank2 and Homer1 are associated with glutamate receptor complexes at rat retinal synapses. *J Comp Neurol.* 2004;475:551–563.
34. Sharma RK, O'Leary TE, Fields CM, Johnson DA. Development of the outer retina in the mouse. *Brain Res Dev Brain Res.* 2003;145:93–105.
35. Morgans CW, Zhang J, Jeffrey BG, et al. TRPM1 is required for the depolarizing light response in retinal ON-bipolar cells. *Proc Natl Acad Sci USA.* 2009;106:19174–19178.
36. Koike C, Obara T, Uriu Y, et al. TRPM1 is a component of the retinal ON bipolar cell transduction channel in the mGluR6 cascade. *Proc Natl Acad Sci USA.* 2010;107:332–337.
37. Jaissle GB, May CA, Reinhard J, et al. Evaluation of the rhodopsin knockout mouse as a model of pure cone function. *Invest Ophthalmol Vis Sci.* 2001;42:506–513.
38. Maeda T, Lem J, Palczewski K, Haeseleer F. A critical role of CaBP4 in the cone synapse. *Invest Ophthalmol Vis Sci.* 2005;46:4320–4327.
39. Seeliger MW, Grimm C, Ståhlberg F, et al. New views on RPE65 deficiency: the rod system is the source of vision in a mouse model of Leber congenital amaurosis. *Nat Genet.* 2001;29:70–74.
40. Haeseleer F, Imanishi Y, Maeda T, et al. Essential role of Ca2+-binding protein 4, a Cav1.4 channel regulator, in photoreceptor synaptic function. *Nat Neurosci.* 2007;7:1079–1087.
41. Mansergh F, Orton NC, Vessey JP, et al. Mutation of the calcium channel gene Cacna1f disrupts calcium signaling, synaptic transmission and cellular organization in mouse retina. *Hum Mol Genet.* 2005;14:3035–3046.
42. Masu M, Iwakabe H, Tagawa Y, et al. Specific deficit of the ON response in visual transmission by targeted disruption of the mGluR6 gene. *Cell.* 1995;80:757–765.
43. Wycisk KA, Budde B, Feil S, et al. Structural and functional abnormalities of retinal ribbon synapses due to Cacna2d4 mutation. *Invest Ophthalmol Vis Sci.* 2006;47:3523–3530.
44. Dick O, tom Dieck S, Altrock WD, et al. The presynaptic active zone protein bassoon is essential for photoreceptor ribbon synapse formation in the retina. *Neuron.* 2003;37:775–786.
45. Satz JS, Philp AR, Nguyen H, et al. Visual impairment in the absence of dystroglycan. *J Neurosci.* 2009;29:13136–13146.
46. Takada Y, Vijayasarathy C, Zeng Y, Kjellstrom S, Bush RA, Sieving PA. Synaptic pathology in retinoschisis knockout (Rs1$^{-/y}$) mouse retina and modification by rAAV-Rs1 gene delivery. *Invest Ophthalmol Vis Sci.* 2008;49:3677–3686.
47. Behndig A, Svensson B, Marklund SL, Karlsson K. Superoxide dismutase isoenzymes in the human eye. *Invest Ophthalmol Vis Sci.* 1998;39:471–475.

48. Hashizume K, Hirasawa M, Imamura Y, et al. Retinal dysfunction and progressive retinal cell death in SOD1-deficient mice. *Am J Pathol.* 2008;172:1325–1331.
49. Justilien V, Pang J, Renganathan K, et al. SOD2 knockdown mouse model of early AMD. *Invest Ophthalmol Vis Sci.* 2007;48:4407–4420.
50. Galbinur T, Obolensky A, Berenshtein E, et al. Effect of para-aminobenzoic acid on the course of retinal degeneration in the rd10 mouse. *J Ocul Pharmacol Ther.* 2009;25:475–482.
51. Lu L, Oveson BC, Jo YJ, et al. Increased expression of glutathione peroxidase 4 strongly protects retina from oxidative damage. *Antioxid Redox Signal.* 2009;11:715–724.
52. Sasaki M, Ozawa Y, Kurihara T, et al. Neuroprotective effect of an antioxidant, lutein, during retinal inflammation. *Invest Ophthalmol Vis Sci.* 2009;50:1433–1439.
53. Teoh CY, Davies KJ. Potential roles of protein oxidation and the immunoproteasome in MHC class I antigen presentation: the 'PrOxI' hypothesis. *Arch Biochem Biophys.* 2004;423:88–96.
54. Cai ZP, Shen Z, Van Kaer L, Becker LC. Ischemic preconditioning-induced cardioprotection is lost in mice with immunoproteasome subunit low molecular mass polypeptide-2 deficiency. *FASEB J.* 2008;22:4248–4257.
55. Hayashi T, Faustman DL. NOD mice are defective in proteasome production and activation of NF-κB. *Mol Cell Biol.* 1999;19:8646–8659.
56. Hayashi T, Faustman DL. Selected contribution: association of gender-related LMP2 inactivation with autoimmune pathogenesis. *J Appl Physiol.* 2001;91:2804–2815.
57. Kisselev AF, Akopian TN, Woo KM, Goldberg AL. The size of peptides generated from protein by mammalian 26 and 20 S proteasomes: implications for understanding the degradative mechanism and antigen presentation. *J Biol Chem.* 1999;274:3363–3371.
58. Fricker LD, Snyder SH. Purification and characterization of enkephalin convertase, an enkephalin-synthesizing carboxypeptidase. *J Biol Chem.* 1983;258:10950–10955.
59. Zhou P, Zanelli E, Smart M, David C. Genomic organization and tissue expression of mouse proteasome gene Lmp-2. *Genomics.* 1993;16:664–668.
60. Stohwasser R, Kuckelkorn U, Kraft R, Kostka S, Kloetzel PM. 20S proteasome from LMP7 knock out mice reveals altered proteolytic activities and cleavage site preferences. *FEBS Lett.* 1996;383:109–113.